the society for solid-state and electrochemical science and technology

Journal of The Electrochemical Society

Interionic Energy Transfer in $Y_3Al_5O_{12}$: Ce^{3+}, Pr^{3+}, Cr^{3+} Phosphor

Lei Wang, Xia Zhang, Zhendong Hao, Yongshi Luo, Ligong Zhang, Ruixia Zhong and Jiahua Zhang

J. Electrochem. Soc. 2012, Volume 159, Issue 4, Pages F68-F72.
doi: 10.1149/2.054204jes

Email alerting service Receive free email alerts when new articles cite this article - sign up in the box at the top right corner of the article or click here

To subscribe to *Journal of The Electrochemical Society* go to:
http://jes.ecsdl.org/subscriptions

©2012 ECS - The Electrochemical Society

Journal of The Electrochemical Society, **159** (4) F68-F72 (2012)
0013-4651/2012/159(4)/F68/5/$28.00 © The Electrochemical Society

Interionic Energy Transfer in $Y_3Al_5O_{12}$: Ce^{3+}, Pr^{3+}, Cr^{3+} Phosphor

Lei Wang,[a,b] Xia Zhang,[a,z] Zhendong Hao,[a] Yongshi Luo,[a] Ligong Zhang,[a] Ruixia Zhong,[c] and Jiahua Zhang[a,z]

[a]*State Key Laboratory of Luminescence and Applications, Changchun Institute of Optics, Fine Mechanics and Physics, Chinese Academy of Sciences, Changchun 130033, China*
[b]*College of Physics and Optoelectronics, Taiyuan University of Technology, Taiyuan 030024, China*
[c]*Department of Materials Science and Engineering, Northeastern University at Qinhuangdao Branch, Qinhuangdao 066004, China*

We present an investigation of dynamical processes of nonradiative energy transfer (ET) in $Y_3Al_5O_{12}$:Ce^{3+}, Pr^{3+}, Cr^{3+} phosphor. The analysis based on Inokuti-Hirayama model indicates that the ET from the lowest 5d state of Ce^{3+} to the $^4T_{2g}$ state of Cr^{3+}, and from the state $^1D_2$ of Pr^{3+} to $^4T_{2g}$ state of Cr^{3+} are both governed by electric dipole-dipole interaction. For Pr^{3+} concentration of 0.005 in YAG: Pr^{3+} Cr^{3+} and for Ce^{3+} concentration of 0.01 in YAG: Ce^{3+} Cr^{3+} the rate constant and critical distance are evaluated to be 7.3×10^{-37} cm^6s^{-1} and 0.22 nm for Pr^{3+} - Cr^{3+} ET and 1.03×10^{-36} cm^6s^{-1} and 0.63 nm for Ce^{3+} - Cr^{3+} ET, respectively.
© 2012 The Electrochemical Society. [DOI: 10.1149/2.054204jes] All rights reserved.

Manuscript submitted December 2, 2011; revised manuscript received January 9, 2012. Published January 31, 2012.

Yttrium aluminum garnet ($Y_3Al_5O_{12}$) has been recognized as one of the best phosphor host materials due its good physical and chemical properties, therefore it is hardly to be replaced by other materials in many fields.[1,2] White light-emitting diodes (LEDs) could be produced by blue chip-pumped yellow $Y_3Al_5O_{12}$: Ce^{3+} (YAG:Ce), whereas color rendering index (CRI) of white light made by the complementary blue and yellow emission is deficient due to the lack of red light contribution. Hence, several red phosphors were developed to add into the above mentioned system in order to improve CRI.[3–7] Unfortunately, the extreme difference in degradation between different host phosphors will produce color aberration. Accordingly, the method that energy transfer (ET) from Ce^{3+} to other co-dope emitting red light ions is chosen to improve YAG:Ce^{3+} emission properties.[8,9]

The study of resonant energy transfer (ET) among impurity ions in phosphor material has been widely researched during recent decades, mainly because it can be used to tune the color of emission light. ET would occur between activator/coactivator couples by effective resonant type via a multipolar interaction. According to the Dexter theory,[10] the mechanism of ET basically requires a spectral overlap between the donor emission and the acceptor excitation, in other words, the ET process may occur if there exists a spectral overlap between the donor emission and the acceptor excitation. In YAG host, Ce^{3+} can act as a sensitizer for other ions such as Pr^{3+}, Cr^{3+} through Dexter theory.[11–16] In our preceding work, we have studied Ce^{3+}-Pr^{3+} ET in Ce^{3+} and Pr^{3+} doubly doped YAG.[16]

In this paper, we demonstrate transfer pathway and transfer dynamical processes in Ce^{3+}, Pr^{3+} and Cr^{3+} codoped YAG basing on the experimental measurements of photoluminescence (PL), photoluminescence excitation (PLE) spectra, and fluorescence decay curves.

Experimental

The powder samples have been prepared by conventional solid-state reaction.Y_2O_3, Al_2O_3, CeO_2, Pr_6O_{11} and Cr_2O_3 are mixed in a molar of $(Y_{1-z-y}Ce_zPr_y)_3(Al_{1-x}Cr_x)_5O_{12}$ (x, y and z represent the concentration of Cr^{3+}, Pr^{3+} and Ce^{3+}, respectively), 3 wt% BaF_2 has been added to as the flux. After a good mixing in an agate mortar, the mixture has been sintered at 1500°C for 3 h under a reducing atmosphere. The structure of the final products is characterized by power X-ray diffraction (XRD). The XRD patterns are in good agreement with Joint Committee for Powder Diffraction Standard file 33-040 for YAG. No additional XRD peaks are found, indicating that the dopant ions do not change the structure of the YAG host. PL and PLE spectra are measured at room temperature with a Hitachi Spextra-fluorometer (F-4500). The decay of the fluorescence from Ce^{3+} is measured by an FL920 fluorimeter (Edinburgh Instruments, Livingston, UK) with a hydrogen flash lamp (nF900; Edinburgh Instruments). In fluorescent decay of Pr^{3+} and Cr^{3+} measurements, an optical parametric oscillator (OPO) is used as an excitation source. The signal is detected by a Tektronix digital oscilloscope (TDS 3052).

Results and Discussion

Spectroscopic evidence of ET.— The PL and PLE spectra of $(Y_{0.99}Ce_{0.01})_3Al_5O_{12}$ (a), $(Y_{0.995}Pr_{0.005})_3Al_5O_{12}$ (b), $Y_3(Al_{0.9925}Cr_{0.0075})_5O_{12}$ (c), $(Y_{0.985}Ce_{0.01}Pr_{0.005})_3Al_5O_{12}$ (d), $(Y_{0.99}Ce_{0.01})_3(Al_{0.9925}Cr_{0.0075})_5O_{12}$ (e) $(Y_{0.995}Pr_{0.005})_3(Al_{0.9925}Cr_{0.0075})_5O_{12}$ (f) and $(Y_{0.985}Ce_{0.01}Pr_{0.005})_3(Al_{0.9925}Cr_{0.0075})_5O_{12}$ (g) samples are shown in Figure 1. All the spectra are normalized to maximum intensity. The Ce^{3+} singly doped sample exhibits a well known yellow emitting broad band due to the transition from the lowest-lying 5d state to the 4f ground state, peaking at around 530 nm. The PLE spectrum of the yellow band consists of a group of PLE bands, including a blue PLE band at 470 nm corresponding to the transition from the ground state to the lowest-lying 5d state, and two ultraviolet (UV) PLE bands corresponding to the upper 5d states, located at 340 nm and 230 nm, respectively,[1,2] as shown in Figure 1a. The Pr^{3+} singly doped sample exhibits three groups of emissions of Pr^{3+} upon 288 nm excitation, as shown in Figure 1b. The group in the UV region consists of two strong bands located at 317 nm and 381 nm, which are originated to the transitions from the lowest lying 4f5d state to ^3H_J (J = 4, 5, 6) and the ^3F_J (J = 2, 3, 4) manifolds, respectively.[17] The group in the range of 450 – 600 nm originates from $^3P_0\rightarrow{}^3H_{4,5}$ transitions dominated by a intense blue emission line at 488 nm due to $^3P_0\rightarrow{}^3H_4$ transition. The other group in red originates from $^1D_2\rightarrow{}^3H_4$ transitions dominated by a intense red emission line at 608 nm with a weak satellite line at 640 nm.[18,19] The PLE spectra of the three groups of emissions in Pr^{3+} singly doped sample are identical in the UV spectral range, showing two 4f5d PLE bands located at 288 nm and 238 nm, respectively. In Figure 2c, the principal features of the PLE spectra of the Cr^{3+} singly doped sample are a O^{2-} – Cr^{3+} related charge transfer band (CTB) at about 230 nm and three broad bands peaking at 280 nm, 443 nm and 608 nm, which belong to the spin-allowed electronic transitions from the $^4A_2$ to the $^4T_1$ (4 P), $^4T_1$ (4 F) and $^4T_2$ (4 F) states, respectively. The PL spectra are the typical emissions of Cr^{3+}, which contains a ^2E – $^4A_2$ zero-phonon line peaking at 685 nm and vibronic sidebands.[20,21] In Figure 1d the PL spectrum of Ce^{3+} and Pr^{3+} doubly doped sample contains not only the yellow band of Ce^{3+} but also the intense red lines of Pr^{3+} when only Ce^{3+} is excited at

[z] E-mail: zhangjh@ciomp.ac.cn; xzhang31@yahoo.cn

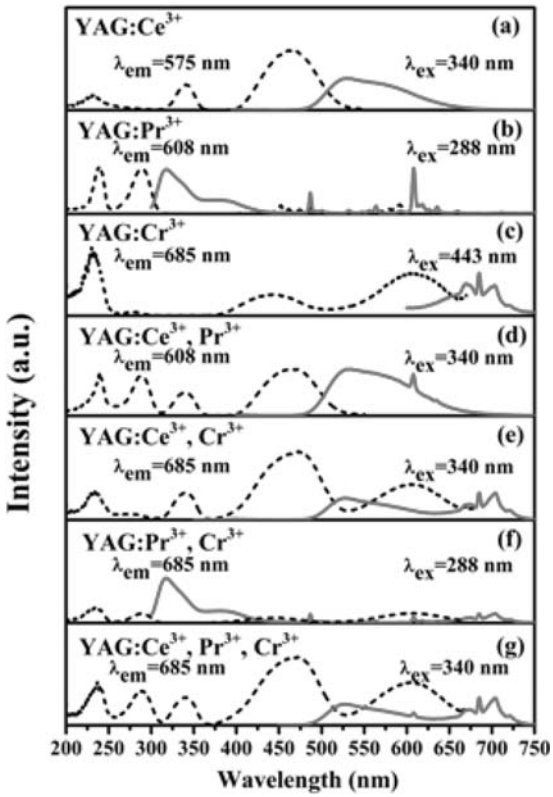

Figure 1. PL and PLE spectra of $(Y_{0.99}Ce_{0.01})_3Al_5O_{12}$ (a), $(Y_{0.995}Pr_{0.005})_3Al_5O_{12}$ (b), $Y_3(Al_{0.9925}Cr_{0.0075})_5O_{12}$ (c), $(Y_{0.985},Ce_{0.01}Pr_{0.005})_3Al_5O_{12}$ (d), $(Y_{0.99}Ce_{0.01})_3(Al_{0.9925}Cr_{0.0075})_5O_{12}$ (e), $(Y_{0.995}Pr_{0.005})_3(Al_{0.9925}Cr_{0.0075})_5O_{12}$ (f) and $(Y_{0.985}Ce_{0.01}Pr_{0.005})_3(Al_{0.9925}Cr_{0.0075})_5O_{12}$ (g).

340 nm, demonstrating occurrence of ET from Ce^{3+} to Pr^{3+}. In Figure 2e, the PL spectrum of Ce^{3+} and Cr^{3+} doubly doped sample contains not only the yellow band of Ce^{3+} but also the red bands of Cr^{3+} when only Ce^{3+} is excited at 340 nm, and furthermore, the PLE spectrum in Figure 2e include the a obvious Ce^{3+} absorption bands at 340 nm and 470 nm when monitored Cr^{3+} 685 nm emission, demonstrating occurrence of energy transfer from Ce^{3+} to Cr^{3+}. Similar to Figure 2e, the PL spectrum of Pr^{3+} and Cr^{3+} doubly doped sample shown in the Figure 2f exhibits three groups of emissions of Pr^{3+} and Cr^{3+} typical emissions at 685 nm as Pr^{3+} is only excited by 288 nm. Compared to the spectra of Pr^{3+} singly doped sample in Figure 2b, the intensity of $^1D_2 \rightarrow {}^3H_4$ emission decline obviously in Figure 2e. Furthermore, the PLE spectra in Figure 2e show a clear Pr^{3+} absorption band at about 288 nm and the tiny sharp line at 488 nm when monitoring Cr^{3+} emission at 685 nm. Figure 2f notably indicates the occurrence of energy transfer from Pr^{3+} to Cr^{3+}. The PL spectrum of Ce^{3+}, Pr^{3+} and Cr^{3+} triply doped sample in Figure 2g exhibits all typical emissions of the three kinds of ions when only Ce^{3+} is excited.

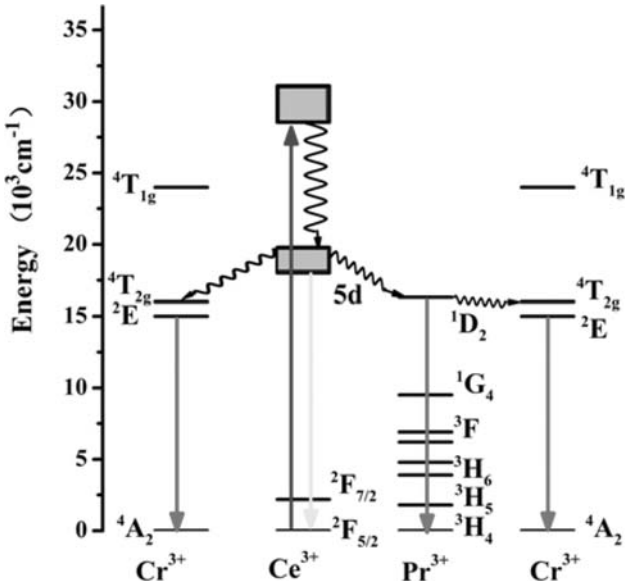

Figure 2. Energy level diagrams of Ce^{3+} Pr^{3+}, and Cr^{3+} with the indicated pathway of energy transfer.

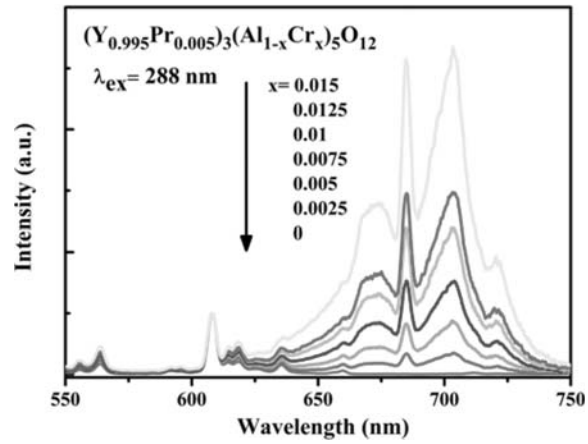

Figure 3. PL spectra of $(Y_{0.995}Pr_{0.005})_3(Al_{1-x}Cr_x)_5O_{12}$, (x = 0, 0.0025, 0.005, 0.0075, 0.01, 0.0125, 0.015) under 288 nm excitation. The intensity of the pale red peak in each spectrum is normalized.

Analysis of fluorescence decay.— Through discussions in section A, there exit Ce^{3+}-Pr^{3+}, Pr^{3+}-Cr^{3+} and Ce^{3+}-Cr^{3+} ET processes in Ce^{3+}, Pr^{3+} and Cr^{3+} triple doped YAG sample. When the upper 5d state of Ce^{3+} is excited at 340 nm, a rapid relaxation down to the lowest 5d state performs and subsequently the energy is transferred from Ce^{3+} to Cr^{3+} and from Ce^{3+} to Pr^{3+}, then Pr^{3+} also transfer energy to Cr^{3+}, as described in the transfer pathway diagrams illustrated in Figure 2. To study these ETs, we prepared the following three series samples. They are series A: $(Y_{0.995}Pr_{0.005})_3(Al_{1-x}Cr_x)_5O_{12}$, series B: $(Y_{0.99}Ce_{0.01})_3(Al_{1-x}Cr_x)_5O_{12}$ and series C: $(Y_{0.985}Ce_{0.01}Pr_{0.005})_3(Al_{1-x}Cr_x)_5O_{12}$ with x in the range from 0 to 0.015.

Firstly, Ce^{3+}-Pr^{3+} ET in Ce^{3+} and Pr^{3+} doubly doped YAG sample has been studied completely in our preceding work.[16]

Secondly, the series A $(Y_{0.995}Pr_{0.005})_3(Al_{1-x}Cr_x)_5O_{12}$ with variable Cr^{3+} concentration x ($x = 0 \sim 0.015$) are synthesized to study the Pr^{3+}-Cr^{3+} ET. Figure 3 shows the PL spectra of sample series A as only Pr^{3+} is excited at 288 nm. All spectra are normalized by the intensity of Pr^{3+} $^1D_2 \rightarrow {}^3H_4$ red line. The PL spectra present enhancement of Cr^{3+} emission with increasing x due to $Pr^{3+} \rightarrow Cr^{3+}$ energy transfer, which also results in shortening of the lifetimes of Pr^{3+} $^1D_2$ as presented in the Figure 4.

Fig. 4 shows the decay curve of red fluorescence of Pr^{3+} in sample series A. The decay is measured by monitoring at 288 nm on 608 nm pulsed excitation. The decays changes from exponential to nonexponential patterns with increasing x, reflecting the effect of ET. The normalized intensity of the donor fluorescence can be written as

$$I_D(t) = I_{D0}(t) f(t), \quad [1]$$

where $I_{D0}(t)$ is the decay function of donors in the absence of acceptors, the function $f(t)$ characterizes the loss of excited donors due to one way ET to the acceptors. If ET rate between a donor and an acceptor is proportional to an inverse power of the distance r, writing as α / r^m,

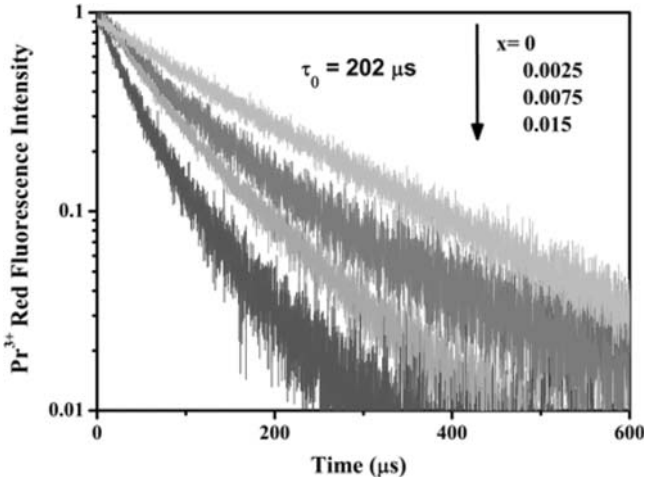

Figure 4. Decay curves of the red line in $(Y_{0.995}Pr_{0.005})_3(Al_{1-x}Cr_x)_5O_{12}$ for x = 0, 0.0025, 0.0075 and 0.015.

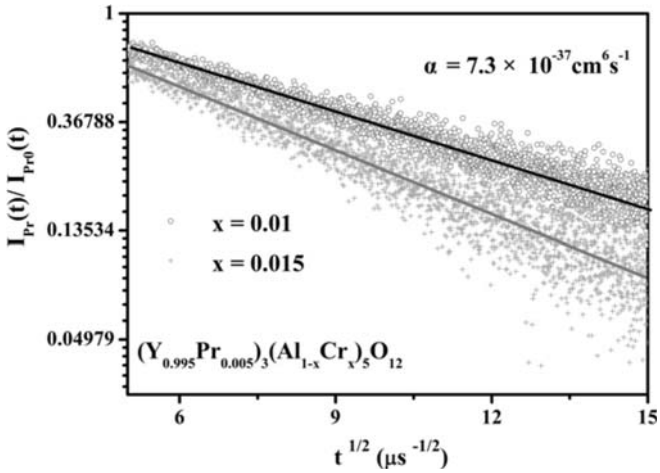

Figure 6. Plotted $\ln[I_{Pr}(t)/I_{Pr0}(t)]$ vs $t^{1/2}$ for the samples$(Y_{0.995}Pr_{0.005})_3(Al_{1-x}Cr_x)_5O_{12}$ with x = 0.01 and 0.015 (b). The solid lines indicate the fitting behaviors.

according to Inokuti-Hirayama formula,[22] we have

$$f(t) = \exp\left[-\frac{4}{3}\pi\Gamma\left(1-\frac{3}{m}\right)n_A\alpha^{3/m}t^{3/m}\right], \qquad [2]$$

where α is a rate constant for ET. m = 6, 8, 10, the coefficient for dipole-dipole, dipole-quadrupole, and quadrupole-quadrupole interaction, respectively. n_A is the number of acceptor ions per unit volume. From Eqs. 1 and 2, $\log\{\ln[I_{D0}(t)/I_D(t)]\}$ acts as a linear function of $\log(t)$ with a slope of $3/m$, and $\ln[I_D(t)/I_{D0}(t)]$ is proportional to $t^{3/m}$ with a slope of $-4\pi\Gamma(1\text{-}3/m)n_A\alpha^{3/m}/3$. Figure 5 shows the log-log plot of $\ln[I_{Pr0}(t)/I_{Pr}(t)]$ vs t for sample $(Y_{0.995}Pr_{0.005})_3(Al_{1-x}Cr_x)_5O_{12}$ with x = 0.01. It is demonstrated that the slope for $t > 50$ μs is 0.52 more close to 1/2, indicating an electric dipole-dipole interaction for ET. Regarding m as 6, we have plotted $\ln[I_{Pr}(t)/I_{Pr0}(t)]$ vs $t^{1/2}$ for the samples $(Y_{0.995}Pr_{0.005})_3(Al_{1-x}Cr_x)_5O_{12}$ with x = 0.01 and 0.015, as shown in Figure 6. The best fitting to each of the two curves yields a transfer constant $\alpha = 7.3\times10^{-37}$ cm^{6}s^{-1}. In the fitting n_A i.e. the number density of Cr^{3+}, is given by xN_{Al} with $N_{Al} = 2.3\times10^{22}$ cm^{-3} being the number of Al sites per unit volume in YAG. Using the value of α the critical ET distance r_0 (the spatial separation between a donor and an acceptor where the ET rate $\alpha/r_0^6 = 1/\tau_{10}$) is calculated to be about 0.22 nm. In the calculation, the $I_{Pr0}(t)$ is an pure exponential decay function $\exp(-t/\tau_{Pr0})$ with $\tau_{pr0} = 202$ μs being the intrinsic lifetime of the $^1D_2$ level of Pr^{3+} in YAG obtained from the tail decay of the fluorescence in 0.001 Pr^{3+} doped YAG.

Figure 7 shows PL spectra of Ce^{3+}, Cr^{3+} doubly doped sample series B (dotted): $(Y_{0.99}Ce_{0.01})_3(Al_{1-x}Cr_x)_5O_{12}$ and triply doped sample series C (solid): $(Y_{0.985}Ce_{0.01}Pr_{0.005})_3(Al_{1-x}Cr_x)_5O_{12}$ with variable Cr^{3+} concentration x in the range of 0 ∼ 0.015 upon Ce^{3+} excitation at 340 nm. All spectra are normalized to the yellow band. The deep red emission of Cr^{3+} grows up with increasing x, reflecting the increase of the $Ce^{3+}\rightarrow Cr^{3+}$ energy transfer efficiency since Cr^{3+} can not be excited directly by 340 nm.

Fig. 8 shows the decay curve of yellow fluorescence of Ce^{3+} in sample series B. The decay is measured by monitoring at 530 nm on 340 nm pulsed excitation. The decays changes from exponential to nonexponential patterns with increasing x, reflecting the effect of ET. The log-log plot of $\ln[I_{Ce0}(t)/I_{Ce}(t)]$ vs t for sample $(Y_{0.99}Ce_{0.01})_3(Al_{1-x}Cr_x)_5O_{12}$ with x = 0.0125 is shown in Figure 9.

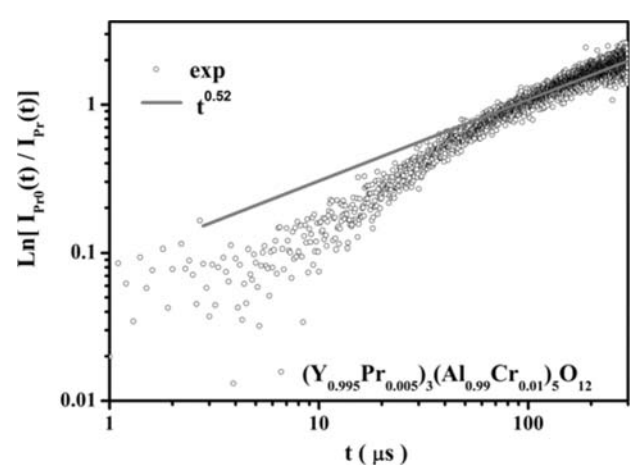

Figure 5. log-log plot of $\ln[I_{Pr0}(t)/I_{Pr}(t)]$ vs t for sample $(Y_{0.995}Pr_{0.005})_3(Al_{1-x}Cr_x)_5O_{12}$ with x = 0.01.

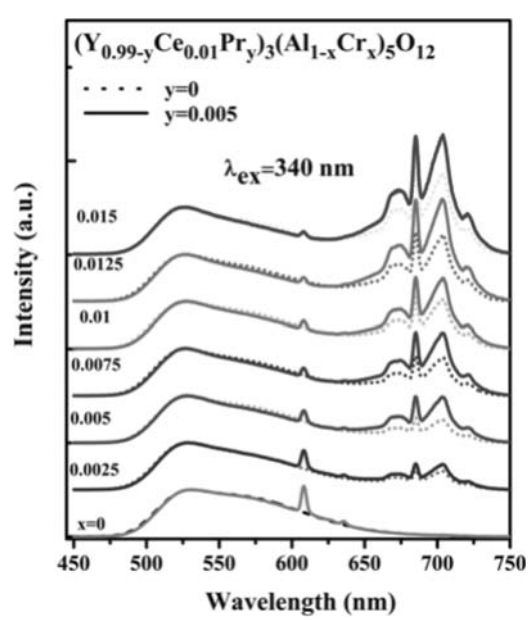

Figure 7. PL spectra of $(Y_{0.99}Ce_{0.01})_3(Al_{1-x}Cr_x)_5O_{12}$, (x = 0, 0.0025, 0.005, 0.0075, 0.01, 0.0125, 0.015; y = 0 (dashed curves), 0.005 (solid curves)) under 340 nm excitation. The intensity of the yellow band in each spectrum is normalized.

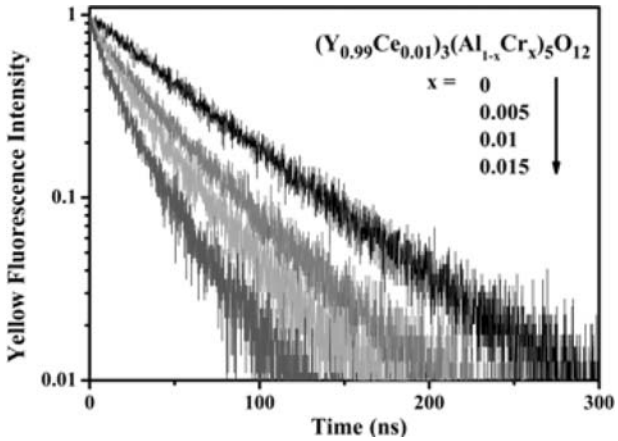

Figure 8. Decay curves of the yellow fluorescence in $(Y_{0.99}Ce_{0.01})_3(Al_{1-x}Cr_x)_5O_{12}$ for x = 0, 0.005, 0.01 and 0.015.

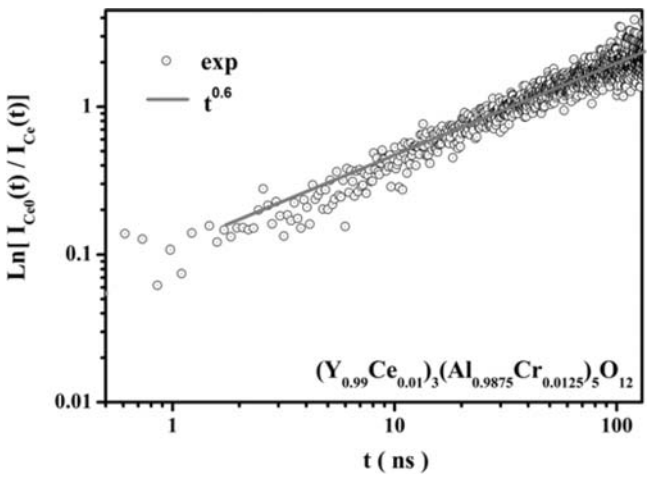

Figure 9. log-log plot of $\ln[I_{Ce0}(t)/I_{Ce}(t)]$ vs t for sample $(Y_{0.99}Ce_{0.01})_3(Al_{1-x}Cr_x)_5O_{12}$ with x = 0.0125.

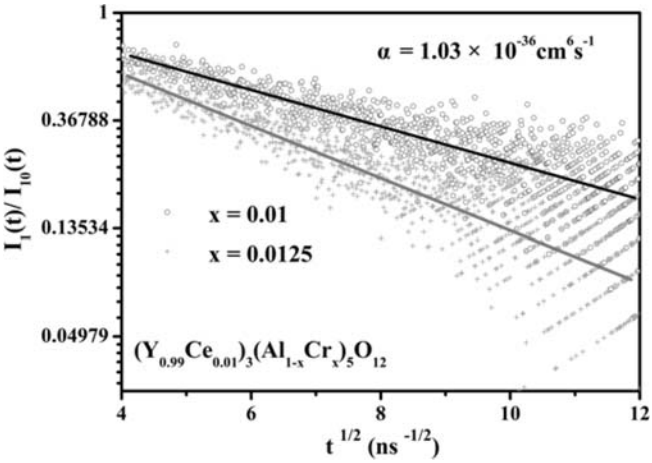

Figure 10. Plotted $\ln[I_{Ce}(t)/I_{Ce0}(t)]$ vs $t^{1/2}$ for the samples $(Y_{0.99}Ce_{0.01})_3(Al_{1-x}Cr_x)_5O_{12}$ with x = 0.01 and 0.0125. The solid lines indicate the fitting behaviors.

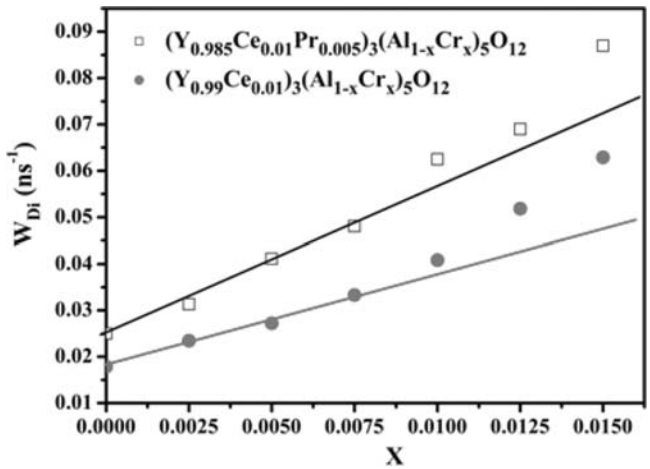

Figure 11. Dependence of W_{Di} on x in $(Y_{0.99}Ce_{0.01})_3(Al_{1-x}Cr_x)_5O_{12}$ and $(Y_{0.985}Ce_{0.01}Pr_{0.005})_3(Al_{1-x}Cr_x)_5O_{12}$.

The slope for $t > 10$ μs is more close to 0.5, indicating an electric dipole-dipole ET between Pr^{3+} ions. The linear dependence of $\ln[I_{Ce}(t)/I_{Ce0}(t)]$ vs $t^{1/2}$ are observed and a good agreement between the theoretical and experimental results are performed for x = 0.01 and 0.0125 when fixing the rate constant α to be 1.03×10^{-36} cm^6s^{-1} for Ce^{3+} - Cr^{3+} ET, as shown in Figure 10. The critical ET distance of 0.63 nm is evaluated.

In Figure 9 there is an increase in slope below 10 ns, forming a crossover.[23] As we know, Eq. 4 is obtained by assuming the nearest distance between a donor and a acceptor to be 0, leading to a infinite initial ET rate. Hence, Eq. 4 is not applicable at short times which is less than 10 ns in the present sample. In the case of discrete lattices, the initial ET rate is described by[24]

$$W_{DAi} = x \sum_l w_{0l}, \quad [3]$$

where w_{0l} is the ET rate from a donor at site 0 to an acceptor at site l excluding $l = 0$. The function f(t), therefore, exhibits a linear behavior $\{f(t) \approx \exp[-W_{DAi}t]\}$ at short times[25] and a $t^{3/m}$ variation at longer times. In random distribution of acceptors in host lattices $\sum_l w_{0l}$ is the averaged ET parameter, denoting the total ET rate of a donor ion embedded within a complete acceptor environment (x = 1). In the present work, the sample for x = 0 shows an exponential decay of fluorescence. Therefore, $\sum_l w_{0l}$ can be experimentally obtained by using the following linear relationship with the initial decay rate W_{Di} of the donor fluorescence[26]

$$W_{Di} = x \sum_l w_{0l} + < \tau_D >_0^{-1} . \quad [4]$$

Figure 11 shows a dependence of W_{Di} on x in sample series B $(Y_{0.99}Ce_{0.01})_3(Al_{1-x}Cr_x)_5O_{12}$ and series C $(Y_{0.985}Ce_{0.01}Pr_{0.005})_3(Al_{1-x}Cr_x)_5O_{12}$ (x = 0 - 0.015). It can be seen a deviation from linear dependence as x higher than 0.0075. It is considered that maybe the Cr^{3+}-Cr^{3+} ion pairs as an acceptor to accept energy when high Cr^{3+} concentration.

Conclusions

Nonradiative energy transfers Ce^{3+}-Pr^{3+}, Pr^{3+}-Cr^{3+} and Ce^{3+}-Cr^{3+} occur in YAG: Ce^{3+}, Pr^{3+}, Cr^{3+} phosphor. When the upper 5d state of Ce^{3+} is excited at 340 nm, a rapid relaxation down to the lowest 5d state performs and subsequently the energy is transferred from Ce^{3+} to $^4T_{2g}$ state of Cr^{3+} and from Ce^{3+} to $^1D_2$ state Pr^{3+}, then Pr^{3+} also transfer energy to Cr^{3+},

Pr^{3+} - Cr^{3+} and Ce^{3+} - Cr^{3+} ET are both governed by electric dipole-dipole interaction. For Pr^{3+} concentration of 0.005 and Ce^{3+} concentration of 0.01, the corresponding rate constant and critical

distance are evaluated to be 7.3×10^{-37} cm^6s^{-1}, 0.22 nm for Ce^{3+} - Pr^{3+} ET and 1.03×10^{-36} cm^6s^{-1}, 0.63 nm for Pr^{3+} - Pr^{3+} ET, respectively.

Acknowledgments

This work is financially supported by the National Nature Science Foundation of China (10834006, 51172226, 10904141, 10904140, 11174278), the MOST of China (2010AA03A404), the Scientific project of Jilin province (20090134, 20090524), CAS Innovation Program and the Major Research Plan of the Natural Science Foundation of Hebei Province, China (grant No. A2010001379).

References

1. G. Blasse and A. Bril, *Appl. Phys. Lett.* **11**, 53 (1967).
2. G. Blasse and A. Bril, *J. Chem. Phys.* **47**, 5139 (1967).
3. R.-J. Xie, N. Hirosaki, M. Nitomo, Y. Yamamoto, T. Suehiro, and K. Sakuma, *J. Phys. Chem. B*, **108**, 12027 (2004).
4. T. Suehiro, N. Hirosaki, R.-J. Xie, and M. Mitimo, *Chem. Mater.*, **17**, 308 (2005).
5. X. Piao, T. Horikawa, H. Hanzawa, and K.-I. Machida, *Chem. Lett.*, **35**, 334 (2006).
6. X. Piao, T. Horikawa, H. Hanzawa, and K.-I. Machida, *Appl. Phys. Lett.*, **88**, 161908 (2006).
7. Y. Q. Li, J. E. J. Van Steen, J. W. H. Van Krevel, G. Botty, A. C. A. Delsing, F. J. DiSalvo, G. de With, and H. T. Hintzen, *J. Alloys Compd.*, **417**, 273 (2006).
8. Yue Tian, et al., *J. Alloy Compd.*, **509**, 6096 (2011).
9. Yanfeng Zheng, et al., *J. Am. Ceram. Soc.*, **94**, 1766 (2011).
10. D. L. Dexter, *J. Chem. Phys.*, **21**, 836 (1953).
11. R. Mueller-Mach, G. O. Mueller, M. R. Krames, and T. Trottier, *IEEE J. Sel. Top. Quantum Electron.*, **8**, 339 (2002).
12. Y. Pan, M. Wu, and Q. Su, *J. Phys. Chem. Solids*, **65**, 845 (2004).
13. H. S. Jang, W. B. Im, D. C. Lee, D. Y. Jeon, and S. S. Kim, *J. Lumin.*, **126**, 371 (2007).
14. H. Yang and Y. S. Kim, *J. Lumin.*, **128**, 1570 (2008).
15. H. Yang, D. K. Lee, and Y. S. Kim, *Mater. Chem. Phys.*, **114**, 665 (2009).
16. Lei Wang, Xia Zhang, Zhendong Hao, Yongshi Luo, Jiahua Zhang, and Xiao-jun Wang, *J. Appl. Phys.*, **108**, 093515 (2010).
17. G. Özen, O. Forte, and B. Di Bartolo, *J. Appl. Phys.*, **97**, 013510 (2005).
18. G. Özen, O. Forte, and B. Di Bartolo, *Opt. Mater.*, **27**, 1664 (2005).
19. M. Malinowski, P. Szczepanski, W. Woliński, R. Wolski, and Z. Frukacz, *J. Phys.: Condens. Matter*, **5**, 6469 (1993).
20. R. Shen and K. L. Bray, *Phys Rev B.*, **56**, 10882 (1997).
21. W. W. Jia, H. Liu, S. Jaffe, W. M. Yen, and B. Denker, *Phys. Rev. B.*, **43**, 5234 (1991).
22. M. Inokuti and F. Hirayama, *J. Chem. Phys.*, **43**, 1978 (1965).
23. P. M. Selzer, D. L. Huber, B. B. Barnett, and W. M. Yen, *Phys. Rev. B.*, **17**, 4979 (1978).
24. M. M. Broer, D. L. Huber, and W. M. Yen, *Phys. Rev. Lett.*, **49**, 394 (1982).
25. D. L. Huber, *Phys. Rev. B.*, **20**, 5333 (1979).
26. W. Lenth, G. Huber, and D. Fay, *Phys. Rev. B.*, **23**, 3877 (1981).